

# Estimating the Color Lifetime of Energetic Quarks

William K. Brooks<sup>a,b,c,\*</sup> and Jorge A. López<sup>a,b,d</sup>

<sup>a</sup>*Departamento de Física, Universidad Técnica Federico Santa María, Valparaíso, Chile*

<sup>b</sup>*Centro Científico Tecnológico de Valparaíso, Valparaíso, Chile*

<sup>c</sup>*Department of Physics and Astronomy, University of New Hampshire, Durham NH, USA*

<sup>d</sup>*Physikalisches Institut, Ruprecht-Karls-Universität Heidelberg, Heidelberg, Germany*

---

## Abstract

A new analysis of published experimental data from the HERMES experiment has been performed. This analysis extracts new information on the space-time properties of color propagation through fitting to a geometric model of the interaction with a realistic nuclear density distribution. Our approach uses a fit to the transverse momentum broadening observable and the hadronic multiplicity ratio; the simultaneous fit to two different observables strongly constrains the outcome. Using the known sizes of the target nuclei, we extract the color lifetime, finding a  $z_h$ -dependent range of values from 2 to 8 fm/c for these data. We also extract estimates for the  $\hat{q}$  transport coefficient characterizing the strength of the interaction between the quark and the cold nuclear medium, finding an average value of  $0.038 \pm 0.026$  GeV<sup>2</sup>/fm. With a two-parameter model we obtain satisfactory fits to the data for the kinematic conditions approximately corresponding to the current fragmentation region. In a secondary fit of the results from that model we independently find a value for the Lund String Model string tension of  $1.04 \pm 0.06$  GeV/fm, consistent with the results from many previous analyses, validating our approach. We evaluated the sensitivity for extracting quark energy loss and effective in-medium hadronic cross sections using three-parameter variants of the model, finding large uncertainties in both cases. Our results suggest that hadronic interaction of forming hadrons in the nuclear medium is the primary dynamical cause of meson attenuation in the HERMES data, with quark energy loss playing a more minor role. The method developed here will be applicable for future data from Jefferson Lab and the Electron Ion Collider.

**Keywords:** Lepto-Nuclear Scattering — Electron-Ion Collider — Lund String Model — Color Confinement — Transport Coefficient — Quark Structure of Nuclei

---

**Introduction.** Data from the highest energy scattering achieved to date continue to be successfully described by perturbative Quantum Chromo Dynamics (pQCD) [1]. Important progress also continues to be made in various non-perturbative sectors and closely related areas, such as lattice QCD [2, 3], AdS/QCD [4, 5, 6], effective field theory [7, 8], and two-particle correlations in collisions of hadronic systems [9, 10]. Over the next decade, breakthrough progress is expected in key areas such as understanding quark confinement in QCD [11, 12].

However, an important soft process with little quantitative progress since the 1970's development of the Lund string model is that of hadronization, despite that this process occurs in every high-energy interaction producing hadronic final states. The hadronization process encodes two fundamental subprocesses: the quasi-free propagation of QCD color charge, not confined within a hadronic bound state; followed by the formation over a finite space-time interval of color-singlet hadrons.

In this paper we analyze data from the HERMES Collaboration [13, 14]. We use a unique new approach that combines two related observables, the transverse momentum broadening and the hadronic multiplicity ratio, to estimate the color lifetime

and the  $\hat{q}$  transport coefficient by comparing data from nuclei of different sizes. We define color lifetime as the duration of time over which a propagating object persists in a state with net color charge<sup>1</sup>. In this work we focus on fundamental processes in the cold matter of atomic nuclei at high Bjorken- $x$  ( $x_{Bj}$ ).

Unlike pQCD cross section calculations, the computation of observables related to the propagation of a parton through a strongly interacting medium is not yet at the stage of precise computations. These studies contain elements of long-distance physics that limit the final precision. Several reviews have appeared over the past two decades [15, 16, 17, 18, 19]. Important quantities which appear in these studies include the transport coefficients  $\hat{q}$  and  $\hat{e}$ , which relate to the transverse momentum broadening and the longitudinal energy loss of partons, respectively. The color lifetime of the propagating parton must be considered in making estimates of the transport coefficients.

---

<sup>1</sup>In older theoretical works, quantities similar to the color lifetime defined here have been referred to as the production time or production length, indicating the time or distance required to form a color singlet object within a particular model approach. We believe color lifetime better represents the significance of this quantity, particularly in the context of in-medium processes, where the color propagation phase can specifically be identified with the transverse momentum broadening, an experimental observable.

---

\*Corresponding author: william.brooks@usm.cl

The HERMES data from the 1990's opened the era of quantitative studies of color propagation in the cold medium by using atomic nuclei as targets for DIS. Such data use the nuclei as spatial analyzers of well-known dimensions, permitting space-time analyses of the data. This opportunity has been anticipated for decades [20, 21], but could not be realized for the measurements preceding HERMES because of the absence of identified hadrons in the final state.

The first HERMES data ruled out several theoretical models. Yet, other models were able to describe the data using approaches with very different dynamical explanations. One approach attributed the origin of the HERMES multiplicity ratio measurements to the energy loss of quarks via gluon bremsstrahlung [22, 23, 24, 25]. The transverse momentum broadening data from HERMES were able to be described in a purely partonic picture [26]. Alternatively, prescriptions were developed that explained the multiplicity ratio data exclusively by interactions of forming hadrons [27, 28] or by a mixture of partonic and hadronic interactions [29, 30]. This controversy remains unresolved. The published models described single observables in one dimension, a natural starting point, but the least stringent test possible. Furthermore, no model exists that describes all of the two-dimensional HERMES data [31], although mesons-only approaches have had some success [32, 30]. Now, prospects for discoveries in our understanding of color propagation are brighter due to new data on semi-inclusive deep inelastic scattering on nuclei (nSIDIS) with identified final-state hadrons. This capability is mandatory for any quantitative studies of the mechanisms involved.

In the present work, we attempt to make progress toward a resolution of this controversy by modeling the data for two observables simultaneously, in one dimension. We also incorporate a realistic nuclear density distribution [33] which we consider to be mandatory for any quantitative comparisons to data. We use a minimum of theoretical assumptions, aiming for a geometrical description in space-time variables, and fit to the data to extract dynamical information. The dynamical behavior, such as the unknown dependence of the color lifetime on the parameter  $z_h \equiv E_h/\nu$  (where  $E_h$  is the hadron energy and  $\nu$  is the energy transfer), is not prescribed by our model but rather emerges from the behavior of the fit in the various kinematic bins for three different nuclei. The model uses the known density distributions of nuclei to extract geometrical information on the color lifetime, on the  $\hat{q}$  transport coefficient, and on the (pre-)hadron inelastic interaction cross section in the medium. It also provides approximate information on the longitudinal energy loss. The aim of this work is to extract basic features of the interaction within simple assumptions.

In our modeling we neglect two-photon exchange [34]. We also neglect the intrinsic momentum of the quark inside the nucleon. In SIDIS for  $x_{Bj} > 0.1$ , the process of quark-antiquark pair production by the virtual photon is negligible [35]. Thus, the full energy and momentum of the virtual photon is absorbed by one valence quark, as shown in Fig. 1. Because the energy and momentum of the virtual photon are measured directly using the scattered lepton, the quark's initial conditions are quite well known, a unique and powerful constraint.

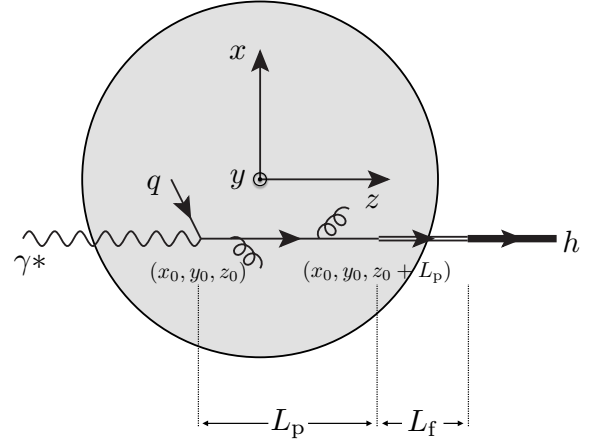


Figure 1: A schematic diagram of the nSIDIS process illustrating our definition of the color length and formation length. The emitted gluons shown are stimulated by multiple scattering in the medium, while the medium-independent gluon emission that would also happen in the vacuum is not shown in the diagram.

**Definition of Characteristic Times and Lengths.** We consider the struck quark moving away from the initial interaction point, traveling as a colored object that emits gluons. After propagating a particular distance, a color singlet system forms from the struck quark and (in the case of a produced meson) an anti-quark, where this  $q\bar{q}$  pair is ultimately contained in the final-state meson. We define the *color length*  $L_c$  as the distance needed to produce the color singlet system. We define the color lifetime  $\tau_c$  as this length divided by the average velocity of the quark, which we take as the speed of light. While we use the concept of length here, it is important to note that the fundamental property is actually a lifetime, which as a time interval would be subject to time dilation if boosted to a different reference frame. We define the formation length  $L_f$  as the additional distance required for the meson to completely form, i.e., to attain its full mass, and the corresponding time as  $\tau_f$ . With these definitions, the total time required to produce a fully formed meson starting from the hard interaction is  $\tau_c + \tau_f$ . In this paper we are measuring  $L_c$ , and from it we can infer  $\tau_c$ . We do not address  $\tau_f$ ; it is only mentioned here for clarity, since some authors use different conventions for these terms [36].

In this work we focus on the hadrons that contain the struck quark. Hadrons with  $z_h > 0.5$  are expected to have a substantially higher probability of containing the struck quark, while hadrons with  $z_h < 0.5$  are expected to be increasingly dominated by target fragmentation kinematics [37, 38].

**Process Modifications Due to the Nuclear Medium.** In the nuclear medium, the above process has two additional features. First, the propagating colored object can interact elastically with the constituents of the medium, stimulating radiative energy loss through additional gluon emission. This has the effect of reducing the quark energy, and broadening the transverse momentum distribution of the quark. As a consequence,

the transverse momentum distribution of the produced hadron is also slightly broader, and on average the produced hadron has slightly less energy. The most basic parameter that represents the color interaction with the medium is the  $\hat{q}$  transport coefficient, which has the operational definition of:

$$\hat{q} = \frac{dp_\perp^2}{d\ell} \Big|_{\text{density-weighted average}} \quad (1)$$

where  $p_\perp$  is the medium-induced part of the parton transverse momentum and  $\ell$  is the longitudinal coordinate along the parton's path. The  $\hat{q}$  transport coefficient is in general a function of multiple variables such as energy and virtuality [39]. Transverse momentum broadening is sensitive to the nuclear quark-gluon correlation functions [40, 41] and thus  $\hat{q}$  is an important probe of the quark structure of atomic nuclei. Efforts are underway to calculate this quantity using lattice QCD [42] in the hot matter environment, but not yet in cold matter. In the standard formulation of in-medium color interactions, the partonic energy loss and the transverse momentum broadening are both proportional to  $\hat{q}$  [15], highlighting its central importance in color propagation studies. In the BDMPS-Z formulation<sup>2</sup> there is a critical parton path length and a critical parton energy [17] which are interrelated. For path lengths less than the critical length, the nominal equation describing the connection to light quark radiative energy loss is:

$$\Delta E = \frac{\alpha_s N_c}{4} \hat{q} \langle L_c^{\text{in-medium}} \rangle^2 \quad (2)$$

The second feature due to the medium is that the produced prehadron can interact with the constituents of the medium. At the hadron energies relevant to this study, the inelastic cross section dominates the elastic cross section and thus the main effect from the medium is for the prehadron to interact inelastically, producing more hadrons of lower energies than would be observed in the vacuum process. In terms of the  $z_h$  variable defined above, these hadrons tend to emerge at much lower  $z_h$ . In the vacuum process at the energies considered here, on average only a few hadrons are produced in a given event; an inelastic interaction with the nuclear medium may produce a hadronic cascade, in which case on average the original value of  $z_h$  will be reduced by a factor of a few, shifting the spectrum to much lower  $z_h$  values for events where these interactions occur.

*Theoretical Expectations.* According to the simplest possible estimates, the path length traveled by the struck quark in a nSIDIS interaction is longer than the dimensions of any nucleus at sufficiently high energies [43]. We suggest that this is only an approximation, even at the highest energies. As an illustration, the Lund string model [44] predicts (see supplementary material) that the color lifetime approaches a small constant at the higher limit of the variable  $z_h = E_h/\nu$  typically used in data analyses. The color lifetime for the struck quark has the following form:

$$\tau_c = \frac{1}{2\beta_{CK}} (M_P + \nu + \sqrt{\nu^2 + Q^2} - 2\nu z_h) \quad (3)$$

In the limit that  $\nu^2 \gg Q^2$ , which is valid for the data we are using, the equation simplifies to

$$\tau_c \rightarrow \frac{1}{2\beta_{CK}} (M_P + 2\nu(1 - z_h)) \quad (\nu^2 \gg Q^2) \quad (4)$$

At high  $z_h$ , for  $\beta_C = 1$ , this becomes

$$\tau_c \rightarrow \frac{M_P}{2K} < 0.5 \text{ fm} \quad (\nu^2 \gg Q^2, z_h \rightarrow \text{large values}) \quad (5)$$

Equivalent behavior is seen when using the closely related lightcone formulation of  $z = p_h^+/P^+$  instead of  $z_h$  (see supplementary materials). This illustrates that in the conventional LSM formulation of Eq. 3, at high  $z_h$  and large  $\nu$  the color lifetime is smaller than the size of any nucleus, independent of other kinematic conditions, and so the struck quark can form a hadron within the nuclear medium even at high energies. The rate of such events is only limited by the relatively low values of the fragmentation function at high  $z_h$  for higher energies. The  $z_h \rightarrow 1$  limit may heuristically be thought of as a consequence of energy conservation, since no gluons could have been emitted by a quark that carries 100% of the available energy, thus the hadron is formed very rapidly on average, and the color lifetime nearly vanishes [45]. Equations 3-5 are not used in our analysis, however, they can be compared with what we derive from the HERMES data using our model; as will be shown, we observe a behavior which is quite consistent with Eq. 3. The physical significance of the pathlength vanishing is that the entity interacting with the nucleus in that case is not partonic. This picture reflects the HERMES data for hadron  $p_T$  broadening as defined below, for which the broadening is consistent with zero at high  $z_h$ . It should also be noted that the behavior at high  $z_h$  mentioned above is reproduced in modeling of HERMES data and EMC data in the GiBUU model [46], that is, at high  $z_h$  there is a measure of hadron attenuation predicted even at the 100-280 GeV beam energies of the EMC experiment.

*Experimental Observables.* Two experimental observables are used simultaneously in this study: the transverse momentum broadening and the multiplicity ratio. The transverse momentum broadening experimental observable is defined as the shift in the mean value of the transverse momentum distribution of hadrons in a larger nucleus A relative to a smaller nucleus D:

$$\Delta p_T^2(Q^2, \nu, z_h) \equiv \langle p_T^2(Q^2, \nu, z_h) \rangle \Big|_A - \langle p_T^2(Q^2, \nu, z_h) \rangle \Big|_D \quad (6)$$

This observable is sensitive to the parton-level multiple scattering mentioned above.

The second experimental observable, the hadronic multiplicity ratio, is defined as follows:

$$R_M^h(Q^2, \nu, z_h, p_T) \equiv \frac{\frac{N_h(Q^2, \nu, z_h, p_T)}{N_e(Q^2, \nu)} \Big|_A}{\frac{N_h(Q^2, \nu, z_h, p_T)}{N_e(Q^2, \nu)} \Big|_D} \quad (7)$$

<sup>2</sup>BDMPS-Z represents foundational work performed by Baier, Dokshitzer, Mueller, Peigne, and Schiff, and in parallel by Zakharov, for which all references can be found in Reference [15].

This observable is equal to unity in the absence of all nuclear effects. In the pion data used in this study,  $R_M^h$  is generally less than unity, i.e., a suppression of hadrons is observed.

*Model Approach.* The model used in this work contains parameters that are determined by a simultaneous fit to the HERMES data for transverse momentum broadening and multiplicity ratio. Each fit is performed for a single bin in  $z_h$ . Four bins in  $z_h$  are considered for the neon, krypton, and xenon nuclei, using a combination of helium and deuterium as a reference as described below. The baseline model (BL) has two parameters: the mean color length and a parameter  $q_0$  related to the  $\hat{q}$  function of Equation 1. We also explored variants of the model, such as (1) incorporation of quark energy loss, and (2) fitting to determine the effective hadronic cross section.

The model uses a realistic mass distribution [?] of the Woods-Saxon form to describe the three heavier nuclei. The Monte Carlo technique is used to average over the initial positions of the struck quark in the nucleus, with an interaction probability weighting proportional to the density function. The distribution of color lengths was modeled in two ways: (1) by a decaying exponential function and (2) by a constant value (delta function). A straight line trajectory of the struck quark was assumed, and the integral of density as a function of path length was computed for the color length  $L_c$  and for the hadron pathlength  $l_h$ . Transverse momentum broadening was taken to be proportional to this integral for  $L_c$ , weighted by the  $q_0$  parameter, and suppression due to a hadronic interaction was taken to be proportional to a decaying exponential using the effective hadronic cross section and the hadron pathlength. It was initially assumed that the fit parameters are independent of the nucleus considered. In a subsequent test we relaxed this assumption, and observed very little change in the parameters.

Specifically, the form of the  $p_T$  broadening calculation is given as:

$$\Delta\langle p_T^2 \rangle = q_0 \left\langle \int_{z_0}^{z_0+L_c^*} \rho(x_0, y_0, \ell) d\ell \right\rangle_{x_0, y_0, z_0, L_c} \quad (8)$$

where  $\ell$  is the spatial coordinate of integration along the path of the parton,  $(x_0, y_0, z_0)$  is the coordinate of the hard interaction point,  $q_0$  is a fit parameter related to the  $\hat{q}$  transport coefficient,  $L_c$  is a fit parameter representing the characteristic color length,  $L_c^*$  is the lesser of  $L_c$  or the distance from  $z_0$  to the sphere of integration surface, and  $\rho$  is the nuclear density function. The Monte Carlo distributions are generated uniformly in  $(x, y, z)$  within an integration sphere centered at  $(0, 0, 0)$ ;  $L_c$  is either randomly generated event-by-event as a decreasing exponential or else taken as a constant value; and each  $(x, y, z)$  point is subsequently assigned a weight proportional to the nuclear density at that point. The underlying physical picture assumed in the proportionality of broadening to this integral is that of a classical diffusion equation, as conventionally used in theoretical treatments [47].

The form of the multiplicity ratio is given in the following

equation:

$$\langle R_M \rangle = \left\langle \exp \left( -\sigma \int_{z_0+L_c^*}^{z_{\max}} \rho(x_0, y_0, \ell) d\ell \right) \right\rangle_{x_0, y_0, z_0, L_c} \quad (9)$$

where the symbols are as defined for the previous equation,  $\sigma$  is the effective prehadron-nucleon cross section, and  $z_{\max}$  is the maximum value of the coordinate  $z$  that is still inside the integration sphere. This equation integrates over the hadron pathlength  $l_h$  mentioned earlier.

The fit of these two quantities is performed using MINUIT [48] in one  $z_h$  bin at a time for all of the nuclei. The power of the fit of the multiplicity ratio and the  $p_T$  broadening for all of the nuclei originates in the simultaneous nature of the fit. For example, for fixed  $q_0$  in a specific event, a longer color length  $L_c$  necessarily produces a shorter hadron pathlength  $l_h$ . This will be visible in the fit as more broadening and less hadron attenuation in a given bin in  $z_h$ . Because these observables have a measured characteristic variation for the three heavier nuclei, the fit is strongly constrained.

In a variant of the baseline model described above, quark energy loss is estimated by fitting energy loss as a reduction in energy transfer  $\nu$  which thus references a higher value of  $z_h$  in the fragmentation function, modifying the multiplicity ratio to be smaller due to the pion fragmentation function. An unmodified  $z_h$  distribution from PYTHIA6 [49] was used to represent the fragmentation function. We find the total quark energy loss  $\Delta E$  to be small, as described below. This is consistent with the small value of  $\hat{q}$  we find from the fit, since  $\Delta E$  should be proportional to  $\hat{q}$  as seen in Equation 2. In a second variant of the baseline model, we fitted the effective hadronic cross section instead of fixing it at the experimental  $\pi$ -nucleon values. The resulting values are compatible with the experimentally measured values [50], but have a large uncertainty.

The primary aim of this work is to estimate the color lifetime of the energetic struck quark. In our model, the strongest constraints on this quantity are the shape of the distribution of  $p_T$  broadening vs.  $A^{1/3}$  and the magnitude of the multiplicity ratio. In the case that the color length is much longer than the diameter of the largest nucleus, in this model this distribution  $\Delta p_T^2(A^{1/3})$  simply becomes a linear function proportional to  $A^{1/3}$ . However, if the color length is smaller than the diameter of the largest nucleus, it introduces a curvature and a reduction in the magnitude of this function. Similarly, if the color length is very short, then the colored system turns into a hadron quickly, thus the hadron attenuation seen in the multiplicity ratio is very strong due to the hadronic interaction in the medium. These two effects are illustrated in Fig. 2, where small  $L_c$  is associated with curvature in  $\Delta p_T^2$  and with strong attenuation in  $R_M^h$ . In Fig. 2 one can also see the experimental sensitivity to the distribution of the color lengths. In the bottom row are the results for fixed color lengths, i.e., for each curve the color length is a single value that does not vary event-by-event, for  $p_T$  broadening (lower middle panel) and the multiplicity ratio (lower right panel). The effect of a color length distribution is shown in the upper row in Fig. 2. As can be seen from this figure, the curvature in  $\Delta p_T^2$  persists to much longer average values

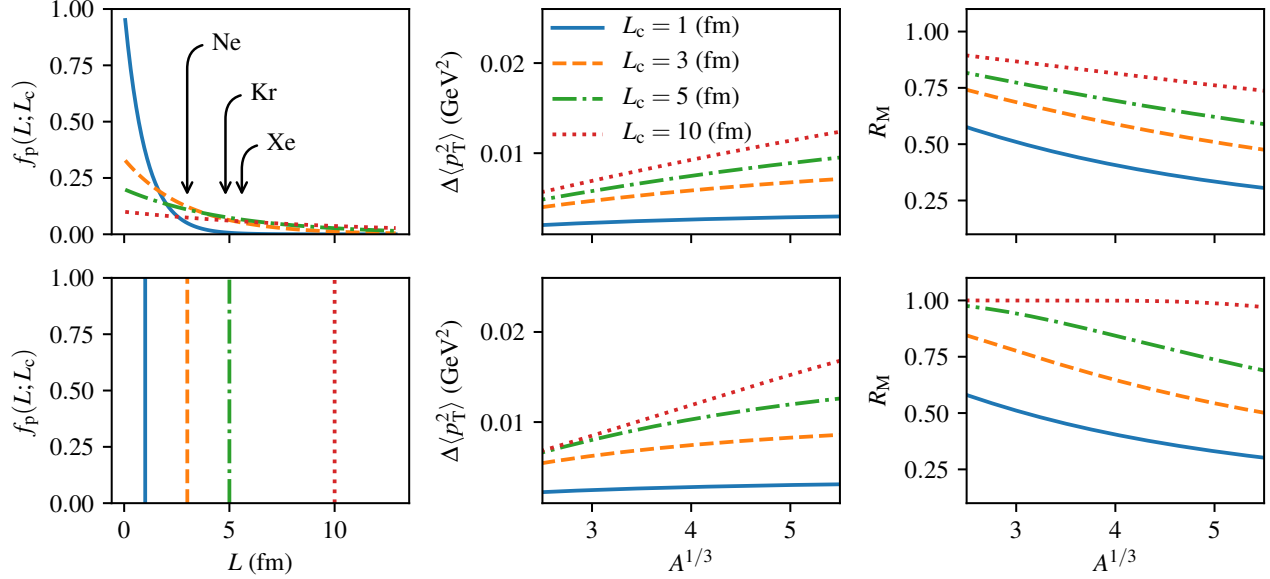


Figure 2: Predictions of this model for  $p_T$  broadening and multiplicity ratio vs.  $A^{1/3}$  for a wide range of values of the color length. In the upper row the color length is distributed according to a decaying exponential distribution as seen in the left-most panel, while in the lower row the calculation assumes a fixed value of the color length for each line, not a distribution of values. The radii for the three heaviest nuclei used in this study are indicated. As can be seen, the differing shapes and magnitudes in the upper and lower rows provide experimental sensitivity to the two classes of distributions which can be used to constrain models of the color lifetime distribution.

of the color length, and the broadening is reduced compared to the case of fixed color length. This is due to the decaying exponential form used in the model for the color length. This demonstrates that there is experimental sensitivity to the form of the color length distribution with precision measurements in the future, as long as multiple nuclei spanning the full range of  $A^{1/3}$  can be compared.

*Treatment of data.* The binning for the HERMES multiplicity ratios is different from that for the  $p_T$  broadening data. Therefore, an interpolation was performed of the multiplicity ratio as a function of  $z_h$  in order to obtain the correct values for the bins to compare to the  $p_T$  broadening data.

One difficulty in using the HERMES data for deuterium as the reference nucleus for  $p_T$  broadening is that the centroid values for several nuclei at higher  $z_h$  are negative, although within the uncertainties they are consistent with zero and with small positive values. We observed that the same was true for the helium data from HERMES. In the simple model we are using it is not conceptually consistent to generate negative values of  $p_T$  broadening. To address this, we took the helium data as being a reference for the deuterium measurements and subtracted the helium centroids from the deuterium centroids.

*Results and Discussion.* Example results of the simultaneous fit to the data for the four  $z_h$  bins are shown in Fig. 3 for the baseline model. In Table 1 the results for two other model variants are shown. The lower fit quality for the lowest value of  $z_h$  in all cases could be due to the limitations of the assumptions of the model, which do not take into account the effects

of hadronic cascades and subleading hadrons, including target fragmentation, which will preferentially populate the low- $z_h$  region of the multiplicity ratio. This table gives both the values of chi-squared per degree of freedom of the fit of the model to the data (center of the table) and the values for the secondary fit of the model results to analytical formulae (right side of the table).

In the following we report on the fit parameters found. First, the estimates for the color length  $L_c$  are shown in Fig. 4 for the baseline model. The horizontal axis is shown as  $z$  and not  $z_h$  to compare the data to theoretical formulations, and the horizontal uncertainties represent the shift between these two related quantities (see supplementary material). We find this parameter to range from 2 to 8 fm for the HERMES data. We find the dependence on  $z_h$  to be compatible with the form given by the Lund string model in Eq. 3. If we subsequently fit our results to the Lund string model form of Eq. 3, leaving the string constant as a free parameter, we independently find a value that is consistent with the well-established value of 1 GeV/fm, as seen in Fig. 4; Table 1 gives the fitting results for the baseline model and two model variants. We consider this agreement to be a powerful validation of our method.

Next, in Fig. 5, we show values of the averaged  $\hat{q}$ , the parameter that specifies the quark-level broadening due to final-state partonic multiple scattering, introduced in Equation 1. At least two different phenomena can contribute to the  $\Delta p_T^2$  measurement. To illustrate this, one can use Equation 2 in reference [52] and reproduced here:

$$\vec{p}_T = z\vec{k}_\perp + \vec{p}_\perp \quad (10)$$

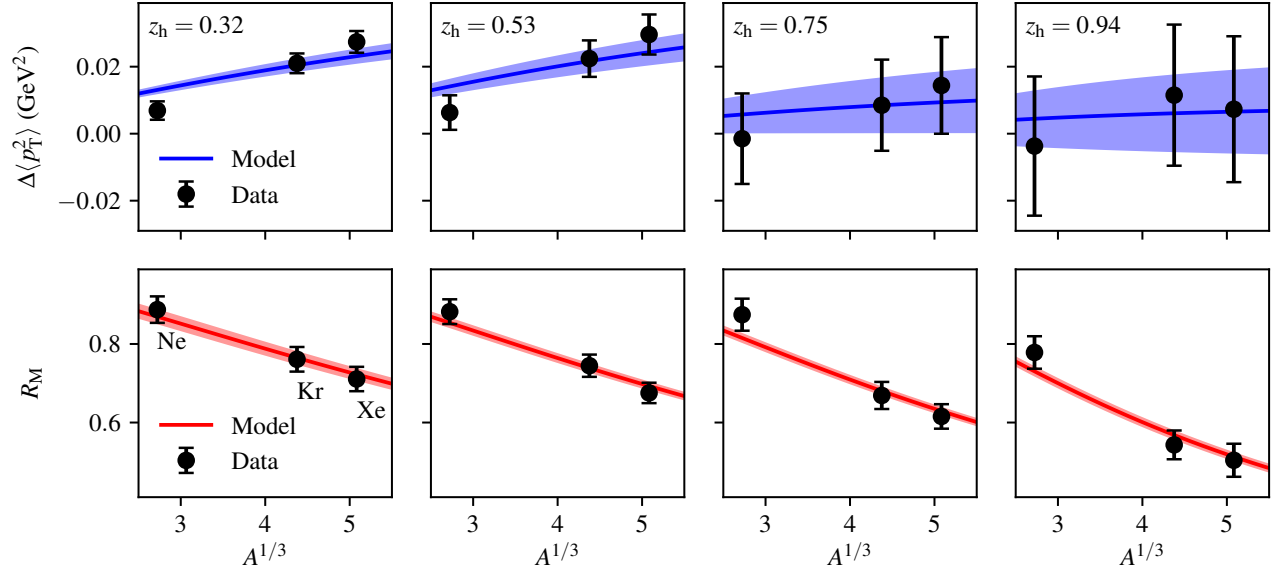


Figure 3: Model function for  $\Delta p_T^2$  (upper panels) and  $R_M^h$  (lower panels) resulting from the simultaneous fit, using the baseline model. The four columns, from left to right, correspond to average values of  $z_h$  of 0.32, 0.53, 0.75, and 0.94, respectively. The six data points from each  $z_h$  bin are fitted simultaneously. The data points shown are from the HERMES experiment, as described in the text. The error bands on the curves represent the fit uncertainty propagated to the observables through analytical expressions derived from Equation 8 and Equation 9.

Table 1: Results from fits to the data and to analytical expressions for the color length that are connected to the Lund String Model. The label “struck quark” refers to Equation 3 (see supplementary materials). The label “B&G” refers to a 1987 paper by Bialas and Gyulassy [51].

Model Variant	Free parameters	$\chi^2/\text{dof}$ of fit to data vs. $z_h$				Fit of results to LSM analytical forms		
		0.32	0.53	0.75	0.94	Analytical form	$\kappa$ (GeV/fm)	$\chi^2/\text{dof}$
Baseline Model	2	1.8	1.1	0.7	0.5	struck quark	$1.04 \pm 0.06$	1.10
with fixed hadronic cross-section						B&G	$0.86 \pm 0.05$	0.35
Baseline Model	3	2.3	1.5	0.9	0.7	struck quark	$1.02 \pm 0.36$	0.08
with free hadronic cross-section						B&G	$0.88 \pm 0.31$	0.15
Baseline Model	3	2.4	1.3	0.5	0.3	struck quark	$1.23 \pm 0.09$	0.16
with quark energy loss						B&G	$1.09 \pm 0.08$	1.09

where  $\vec{p}_T$  is the transverse momentum of the produced hadron,  $\vec{k}_\perp$  is the intrinsic transverse momentum of the quark, and  $\vec{p}_\perp$  is the transverse momentum of the hadron  $h$  with respect to the direction  $k'$  of the fragmenting quark. In the vacuum process [53],

$$\langle p_T^2 \rangle \approx \langle k_\perp^2 \rangle \cdot z_h^2 + \langle p_\perp^2 \rangle \quad (11)$$

and thus in the medium, comparing two nuclei  $D$  and  $A$  of different sizes,

$$\Delta p_T^2 \equiv p_{T|A}^2 - p_{T|D}^2 \approx \Delta k_\perp^2 \cdot z_h^2 + \Delta p_\perp^2 \quad (12)$$

where the final hadron transverse momentum broadening has two components: a broadening term depending on the initial state  $k_\perp$  distribution that scales with  $z_h^2$ , and a broadening term that depends on the final state fragmentation process and which thus reflects interactions with the nuclear medium. Since the distribution of *longitudinal* momentum fraction  $x_{Bj}$  is known to

be modified in bound nucleons, as observed in the well-known EMC effect [54, 55, 56], it is expected that there is also a corresponding modification in the initial state *transverse* momentum distribution. Thus,  $\Delta k_\perp^2$  may be different from zero when comparing nuclei of different sizes, an effect that may become apparent in studies of future data of higher precision. In particular, this line of reasoning clearly predicts the existence of a dependence on  $x_{Bj}$  for  $\Delta k_\perp^2$  and thereby also for  $\Delta p_T^2$ ; naively, for mid- $x_{Bj}$ ,  $\Delta k_\perp^2$  may actually be less than zero if it follows the EMC effect pattern of reduced valence quark momentum in nuclei. More precise data are needed to evaluate whether  $\Delta k_\perp^2$  can be estimated from data using its dependence on  $x_{Bj}$  and  $z_h$ . A dependence on  $x_{Bj}$  was recently observed in the analysis of [57] and interpreted as an  $x_{Bj}$  dependence of the jet transport coefficient. A dependence of pion  $p_T$  broadening on  $x_{Bj}$  and  $Q^2$  was predicted from pQCD two decades earlier [58].

Our model does not contain  $\Delta k_\perp^2$ , thus, we estimate  $\hat{q}$  in the

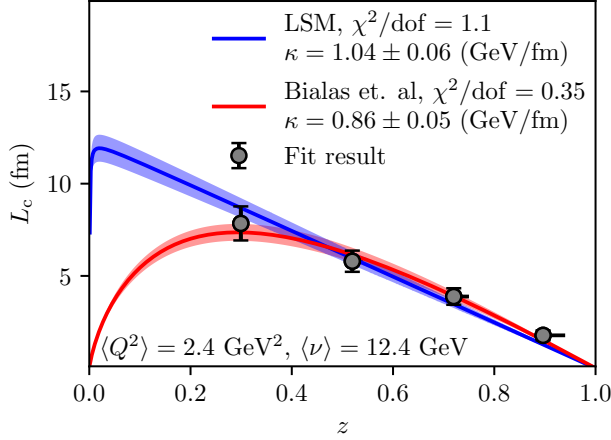


Figure 4: The values of the color length resulting from the transverse momentum broadening and multiplicity ratio simultaneous fit. The results of the baseline model fit are shown with solid circles, and the errors bars represent the model fit uncertainty. Fits of the color length parameter to predictions from the Lund string model are shown in red and blue with shaded areas representing the uncertainties of this secondary fit. The horizontal uncertainties represent the shift due to changing from  $z_h$  to  $z$  for comparing data to theoretical formulations. The curve labeled LSM is Equation 3 (see supplementary material), while the curve labeled Bialas is from a 1987 paper by Bialas and Gyulassy [51].

approximation that  $\Delta p_T^2 \approx \Delta p_\perp^2$ . The value for  $\hat{q}$  found in our model is approximately  $0.04 \text{ GeV}^2/\text{fm}$ , and within the fit uncertainties there is no dependence on the nuclear size, as seen in Fig. 5. This value is compatible with the results of a recently published global analysis that included the HERMES data [57]. It is also compatible with an extraction from E866 Drell-Yan data of the *gluon* transport coefficient at  $\sqrt{s} = 38.7 \text{ GeV}$  [59] of  $0.075^{+0.015}_{-0.05} \text{ GeV}^2/\text{fm}$  which was used to describe proton-lead collision data at  $\sqrt{s} = 5 \text{ TeV}$  [60]; to compare to our result for the *quark* transport coefficient, it is necessary to correct for the color factor of 9/4, resulting in  $0.033^{+0.007}_{-0.02}$ , in excellent agreement with our results. However, our value is significantly smaller than that found from a study of the HERMES data from 2015 [61] which obtained a value of  $0.74 \pm 0.03 \text{ GeV}^2/\text{fm}$ .

In the baseline model we include the experimentally measured pion-nucleon cross section. In the model variant where that cross section is a fit parameter, our results for the hadronic cross section are basically independent of  $z_h$  and are quite consistent with published pion-nucleon cross sections [50]. We find an average value for  $z_h > 0.5$  of 22 mbarn, however, the fit uncertainties are greater than 50%, thus they are also compatible with a reduced cross section as might be expected for forming hadrons.

For fits that included quark energy loss, the value found was small, at a level of 200 MeV or less, with uncertainties exceeding 500 MeV. The inclusion of quark energy loss did not uniformly improve the fits to the data, as can be seen in Table 1. This observation is not surprising because we also find  $\hat{q}$  to be quite small; using Eq. 2 one can easily verify that the change in  $z_h$  caused by an energy loss corresponding to  $\hat{q} \approx 0.04 \text{ GeV}^2/\text{fm}$  must be almost negligible compared to the widths of the four

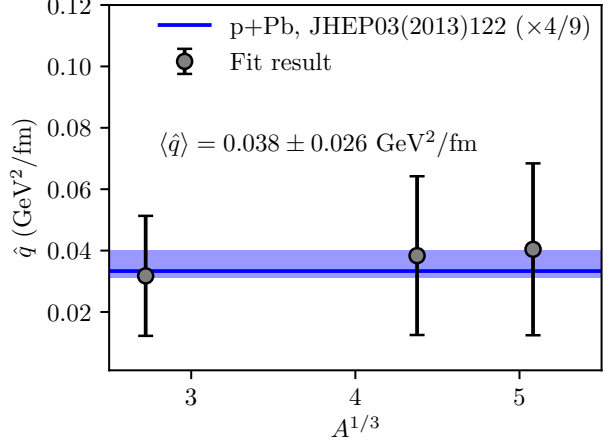


Figure 5: The values of the transport coefficient  $\hat{q}$  for neon, krypton and xenon resulting from the transverse momentum broadening and multiplicity ratio simultaneous fit. The error bars represent the fit uncertainty. The factor of 4/9 applied to the published data is the color factor relating gluon-medium interactions to quark-medium interactions.

experimental  $z_h$  bins, thus, these data do not have enough precision to determine quark energy loss accurately in our approach. As a general pattern, phenomenological approaches that seek to explain the multiplicity ratio entirely by quark energy loss result in larger values of  $\hat{q}$ , which then tends to cause a tension with the small measured values of  $p_T$  broadening. This reinforces the value of the simultaneous fit to the two observables that we have performed here.

**Summary and Conclusions.** We have used HERMES data to estimate the color lifetime of the struck quark in semi-inclusive deep inelastic scattering on nuclei. The dynamical behavior is not prescribed by our model but rather emerges from the behavior of the fit in the various kinematic bins for three different nuclei. The interactions with the nuclear medium of the struck quark, and the subsequent forming hadron that contains it, reveal the details of the color propagation and hadron formation process at the femtometer scale. We defined the important elements of the physical picture within a simple geometric framework that primarily relies on the well-known density distributions of heavier nuclei. We performed simultaneous fits of two observables: the multiplicity ratio and the transverse momentum broadening. We explored fits within this framework that had either two or three free parameters, always including the color lifetime and a quark-medium interaction parameter related to the  $\hat{q}$  transport coefficient, and as variants including an hadronic interaction cross section to represent interactions between the medium and forming hadron, and the total energy loss of the struck quark in the medium. The result for the color length was stable in all model variants and ranged from 2 fm to 8 fm for the HERMES data, depending on the relative energy fraction  $z_h$  of the formed hadron. Within this framework we independently estimated the Lund String Model string tension  $\kappa$  to be  $1.04 \pm 0.06 \text{ GeV/fm}$  using the baseline model alone,



and  $1 \pm 0.2$  GeV/fm using the baseline model together with two model variants, in good agreement with historical determinations, which strongly validates our approach. We also found there can be experimental sensitivity to the analytical form of the distribution of the color lifetime as shown in Fig. 2, which can be used in more precise data in the future to constrain and characterize this function.

**Acknowledgements.** We gratefully acknowledge productive discussions with B. Z. Kopeliovich, S. Brodsky, J. Qiu, A. Majumder, T. Sjöstrand, S. Peigné, M. Boglione, and R. Ent who were instrumental in our development and validation of the concepts for this model. We further acknowledge partial financial support from the following Chilean grants: CONICYT PIA ACT-1413, ACT-1409, BASAL FB-0821; FONDECYT 1080564, 1120953, and 1161642; Beca CONICYT Doctorado Nacional 2014 21140777, UTFSM DGIIP PIIC 2015 and 2017, ECOS-CONICYT C12E04. This work was initiated from discussions in 2009 during the US Institute for Nuclear Theory Program INT-09-3 and workshop INT-09-43W at the University of Washington.

## References

- [1] M. Aaboud, G. Aad, B. Abbott, O. Abidinov, B. Abeloos, S. H. Abidi, O. S. AbouZeid, N. L. Abraham, H. Abramowicz, et al., Measurement of inclusive jet and dijet cross-sections in proton-proton collisions at  $\sqrt{s} = 13$  TeV with the ATLAS detector, *Journal of High Energy Physics* 2018 (5). doi:10.1007/jhep05(2018)195. URL [http://dx.doi.org/10.1007/JHEP05\(2018\)195](http://dx.doi.org/10.1007/JHEP05(2018)195)
- [2] R. A. Briceo, J. J. Dudek, R. G. Edwards, D. J. Wilson, Isoscalar  $\pi\pi$  Scattering and the  $\sigma$  Meson Resonance from QCD, *Physical Review Letters* 118 (2). doi:10.1103/physrevlett.118.022002. URL <http://dx.doi.org/10.1103/PhysRevLett.118.022002>
- [3] S. R. Beane, E. Chang, W. Detmold, K. Orginos, A. Parreno, M. J. Savage, B. C. Tiburzi, Ab initio Calculation of the  $np \rightarrow dy$  Radiative Capture Process, *Phys. Rev. Lett.* 115 (13) (2015) 132001. arXiv:1505.02422, doi:10.1103/PhysRevLett.115.132001.
- [4] S. J. Brodsky, G. F. de Teramond, H. G. Dosch, J. Erlich, Light-Front Holographic QCD and Emerging Confinement, *Phys. Rept.* 584 (2015) 1–105. arXiv:1407.8131, doi:10.1016/j.physrep.2015.05.001.
- [5] T. Gutsche, V. E. Lyubovitskij, I. Schmidt, A. Vega, Nuclear physics in soft-wall AdS/QCD: Deuteron electromagnetic form factors, *Phys. Rev. D* 91 (11) (2015) 114001. arXiv:1501.02738, doi:10.1103/PhysRevD.91.114001.
- [6] T. Gutsche, V. E. Lyubovitskij, I. Schmidt, A. Vega, Nucleon structure in a light-front quark model consistent with quark counting rules and data, *Phys. Rev. D* 91 (2015) 054028. arXiv:1411.1710, doi:10.1103/PhysRevD.91.054028.
- [7] N. Barnea, L. Contessi, D. Gazit, F. Pederiva, U. van Kolck, Effective Field Theory for Lattice Nuclei, *Phys. Rev. Lett.* 114 (5) (2015) 052501. arXiv:1311.4966, doi:10.1103/PhysRevLett.114.052501.
- [8] C. Ji, C. Elster, D. R. Phillips,  $^6\text{He}$  nucleus in halo effective field theory, *Phys. Rev. C* 90 (4) (2014) 044004. arXiv:1405.2394, doi:10.1103/PhysRevC.90.044004.
- [9] G. Aad, et al., Observation of Long-Range Elliptic Azimuthal Anisotropies in  $\sqrt{s} = 13$  and 2.76 TeV  $pp$  Collisions with the ATLAS Detector, *Phys. Rev. Lett.* 116 (17) (2016) 172301. arXiv:1509.04776, doi:10.1103/PhysRevLett.116.172301.
- [10] L. Adamczyk, et al., Measurement of elliptic flow of light nuclei at  $\sqrt{s_{NN}} = 200, 62.4, 39, 27, 19.6, 11.5$ , and 7.7 GeV at the BNL Relativistic Heavy Ion Collider, *Phys. Rev. C* 94 (3) (2016) 034908. arXiv:1601.07052, doi:10.1103/PhysRevC.94.034908.
- [11] H. Al Ghoul, et al., First Results from The GlueX Experiment, AIP Conf. Proc. 1735 (2016) 020001. arXiv:1512.03699, doi:10.1063/1.4949369.
- [12] I. G. Aznauryan, et al., Studies of Nucleon Resonance Structure in Exclusive Meson Electroproduction, *Int. J. Mod. Phys. E* 22 (2013) 1330015. arXiv:1212.4891, doi:10.1142/S0218301313300154.
- [13] A. Airapetian, et al., Transverse momentum broadening of hadrons produced in semi-inclusive deep-inelastic scattering on nuclei, *Phys. Lett. B* 684 (2010) 114–118. arXiv:0906.2478, doi:10.1016/j.physletb.2010.01.020.
- [14] A. Airapetian, et al., Hadronization in semi-inclusive deep-inelastic scattering on nuclei, *Nucl. Phys. B* 780 (2007) 1–27. arXiv:0704.3270, doi:10.1016/j.nuclphysb.2007.06.004.
- [15] R. Baier, D. Schiff, B. G. Zakharov, Energy loss in perturbative QCD, *Ann. Rev. Nucl. Part. Sci.* 50 (2000) 37–69. arXiv:hep-ph/0002198, doi:10.1146/annurev.nucl.50.1.37.
- [16] S. A. Bass, M. Gyulassy, H. Stoecker, W. Greiner, Signatures of quark gluon plasma formation in high-energy heavy ion collisions: A Critical review, *J. Phys. G* 25 (1999) R1–R57. arXiv:hep-ph/9810281, doi:10.1088/0954-3899/25/3/013.
- [17] S. Peigne, A. V. Smilga, Energy losses in a hot plasma revisited, *Phys. Usp.* 52 (2009) 659–685, [*Usp. Fiz. Nauk* 179.697(2009)]. arXiv:0810.5702, doi:10.3367/UFNe.0179.200907a.0697.
- [18] A. Accardi, F. Arleo, W. K. Brooks, D. D’Enterria, V. Muccifora, Parton Propagation and Fragmentation in QCD Matter, *Riv. Nuovo Cim.* 32 (2010) 439–553. arXiv:0907.3534, doi:10.1393/ncr/i2009-10048-0.
- [19] A. Majumder, M. Van Leeuwen, The Theory and Phenomenology of Perturbative QCD Based Jet Quenching, *Prog. Part. Nucl. Phys.* 66 (2011) 41–92. arXiv:1002.2206, doi:10.1016/j.pnpnp.2010.09.001.
- [20] S. J. Brodsky, A. H. Mueller, Using Nuclei to Probe Hadronization in QCD, *Phys. Lett. B* 206 (1988) 685–690. doi:10.1016/0370-2693(88)90719-8.
- [21] Gyulassy, Miklos and Wang, Xin-nian, Multiple collisions and induced gluon Bremsstrahlung in QCD, *Nucl. Phys. B* 420 (1994) 583–614. arXiv:nuc1-th/9306003, doi:10.1016/0550-3213(94)90079-5.
- [22] N.-B. Chang, W.-T. Deng, X.-N. Wang, Initial conditions for the modified evolution of fragmentation functions in the nuclear medium, *Physical Review C* 89 (3). doi:10.1103/physrevc.89.034911. URL <http://dx.doi.org/10.1103/PhysRevC.89.034911>
- [23] G.-Y. Qin, A. Majumder, Parton transport via transverse and longitudinal scattering in dense media, *Physical Review C* 87 (2). doi:10.1103/physrevc.87.024909. URL <http://dx.doi.org/10.1103/PhysRevC.87.024909>
- [24] A. Majumder, The in-medium scale evolution in jet modification (2009). arXiv:0901.4516.
- [25] F. Arleo, Quenching of hadron spectra in DIS on nuclear targets, *The European Physical Journal C* 30 (2) (2003) 213221. doi:10.1140/epjc/s2003-01289-x. URL <http://dx.doi.org/10.1140/epjc/s2003-01289-x>
- [26] S. Domdey, D. Grnewald, B. Kopeliovich, H. Pirner, Transverse momentum broadening in semi-inclusive DIS on nuclei, *Nuclear Physics A* 825 (3-4) (2009) 200211. doi:10.1016/j.nuclphysa.2009.04.009. URL <http://dx.doi.org/10.1016/j.nuclphysa.2009.04.009>
- [27] T. Falter, W. Cassing, K. Gallmeister, U. Mosel, Hadron formation and attenuation in deep inelastic lepton scattering off nuclei, *Physics Letters B* 594 (1-2) (2004) 6168. doi:10.1016/j.physletb.2004.04.089. URL <http://dx.doi.org/10.1016/j.physletb.2004.04.089>
- [28] K. Gallmeister, U. Mosel, Time dependent hadronization via HERMES and EMC data consistency, *Nuclear Physics A* 801 (1-2) (2008) 6879. doi:10.1016/j.nuclphysa.2007.12.009. URL <http://dx.doi.org/10.1016/j.nuclphysa.2007.12.009>
- [29] B. Kopeliovich, J. Nemchik, E. Predazzi, A. Hayashigaki, Nuclear hadronization: within or without?, *Nuclear Physics A* 740 (1-2) (2004) 211245. doi:10.1016/j.nuclphysa.2004.04.110. URL <http://dx.doi.org/10.1016/j.nuclphysa.2004.04.110>
- [30] B. Guiot, B. Kopeliovich, Spacetime development of in-medium hadronization: Scenario for leading hadron, arXiv:2001.00974.
- [31] A. Airapetian, N. Akopov, Z. Akopov, E. C. Aschenauer, W. Augustyniak, R. Avakian, A. Avetissian, E. Avetisyan, S. Belostotski, et al., Multidimensional study of hadronization in nuclei, *The European Physical Journal A* 47 (9). doi:10.1140/epja/i2011-11113-5. URL <http://dx.doi.org/10.1140/epja/i2011-11113-5>
- [32] L.-H. Song, S.-F. Xin, N. Liu, The energy loss and nuclear absorption



- effects in semi-inclusive deep inelastic scattering on nucleus, *J. Phys. G* 45 (2) (2018) 025005. doi:10.1088/1361-6471/aaa09b.
- [33] Blok, H. P. and Lapikás, L., A-dependence of hadronization in nuclei, *Physical Review C* 73 (3). doi:10.1103/physrevc.73.038201. URL <http://dx.doi.org/10.1103/PhysRevC.73.038201>
- [34] D. Adikaram, et al., Towards a resolution of the proton form factor problem: new electron and positron scattering data, *Phys. Rev. Lett.* 114 (2015) 062003. arXiv:1411.6908, doi:10.1103/PhysRevLett.114.062003.
- [35] V. Del Duca, S. J. Brodsky, P. Hoyer, Space-time structure of deep inelastic lepton - hadron scattering, *Phys. Rev. D* 46 (1992) 931–943. doi:10.1103/PhysRevD.46.931.
- [36] L. Grigoryan, Average formation length of hadrons in a string model, *Physical Review C* 81 (4). doi:10.1103/physrevc.81.045207. URL <http://dx.doi.org/10.1103/PhysRevC.81.045207>
- [37] E. L. Berger, SEMI-INCLUSIVE INELASTIC ELECTRON SCATTERING FROM NUCLEI, in: NPAS WORKSHOP ON ELECTRONUCLEAR PHYSICS WITH INTERNAL TARGETS, SLAC, JANUARY 5-8, 1987, 1987, pp. 82–91.
- [38] M. Boglione, A. Dotson, L. Gamberg, S. Gordon, J. O. Gonzalez-Hernandez, A. Prokudin, T. C. Rogers, N. Sato, Mapping the Kinematical Regimes of Semi-Inclusive Deep Inelastic Scattering, *JHEP* 10 (2019) 122. arXiv:1904.12882, doi:10.1007/JHEP10(2019)122.
- [39] A. Kumar, A. Majumder, C. Shen, Energy and scale dependence of  $\hat{q}$  and the JET puzzle, *Physical Review C* 101 (3). doi:10.1103/physrevc.101.034908. URL <http://dx.doi.org/10.1103/PhysRevC.101.034908>
- [40] M. Luo, J. Qui, G. Sterman, Nuclear dependence at large transverse momentum, *Physics Letters B* 279 (3) (1992) 377 – 383. doi:https://doi.org/10.1016/0370-2693(92)90408-V. URL <http://www.sciencedirect.com/science/article/pii/037026939290408V>
- [41] M. Luo, J. Qiu, G. Sterman, Anomalous nuclear enhancement in deeply inelastic scattering and photoproduction, *Phys. Rev. D* 50 (1994) 1951–1971. doi:10.1103/PhysRevD.50.1951. URL <https://link.aps.org/doi/10.1103/PhysRevD.50.1951>
- [42] A. Kumar, A. Majumder, C. Nonaka, First calculation of  $\hat{q}$  on a quenched SU(3) plasma, in: 36th International Symposium on Lattice Field Theory (Lattice 2018) East Lansing, MI, United States, July 22-28, 2018, 2018. arXiv:1811.01329.
- [43] E. Wang, X.-N. Wang, Jet tomography of dense and nuclear matter, *Phys. Rev. Lett.* 89 (2002) 162301. arXiv:hep-ph/0202105, doi:10.1103/PhysRevLett.89.162301.
- [44] B. Andersson, G. Gustafson, G. Ingelman, T. Sjöstrand, Parton Fragmentation and String Dynamics, *Phys. Rept.* 97 (1983) 31–145. doi:10.1016/0370-1573(83)90080-7.
- [45] B. Z. Kopeliovich, L. B. Litov, J. Nemchik, Effects of Formation Time and Colour Transparency on the Production of Leading Particles off Nuclei, *JINR Preprint* E2-90-344. URL [https://inis.iaea.org/collection/NCLCollectionStore/\\_Public/23/051/23051138.pdf](https://inis.iaea.org/collection/NCLCollectionStore/_Public/23/051/23051138.pdf)
- [46] K. Gallmeister, U. Mosel, Time Dependent Hadronization via HERMES and EMC Data Consistency, *Nucl. Phys. A* 801 (2008) 68–79. arXiv:nucl-th/0701064, doi:10.1016/j.nuclphysa.2007.12.009.
- [47] R. Baier, Y. Dokshitzer, A. Mueller, S. Peign, D. Schiff, Radiative energy loss and  $p_{\perp}$ -broadening of high energy partons in nuclei, *Nuclear Physics B* 484 (1-2) (1997) 265282. doi:10.1016/S0550-3213(96)00581-0. URL [http://dx.doi.org/10.1016/S0550-3213\(96\)00581-0](http://dx.doi.org/10.1016/S0550-3213(96)00581-0)
- [48] F. James, M. Roos, Minuit: A System for Function Minimization and Analysis of the Parameter Errors and Correlations, *Comput. Phys. Commun.* 10 (1975) 343–367. doi:10.1016/0010-4655(75)90039-9.
- [49] T. Sjöstrand, S. Mrenna, P. Z. Skands, PYTHIA 6.4 Physics and Manual, *JHEP* 05 (2006) 026. arXiv:hep-ph/0603175, doi:10.1088/1126-6708/2006/05/026.
- [50] M. Tanabashi, K. Hagiwara, K. Hikasa, K. Nakamura, Y. Sumino, F. Takahashi, J. Tanaka, K. Agashe, G. Aielli, C. Amsler, M. Antonelli, D. M. Asner, H. Baer, S. Banerjee, R. M. Barnett, T. Basaglia, C. W. Bauer, J. J. Beatty, V. I. Belousov, J. Beringer, S. Bethke, A. Bettini, H. Bichsel, O. Biebel, K. M. Black, E. Blucher, O. Buchmüller, V. Burkert, M. A. Bychkov, R. N. Cahn, M. Carena, A. Ceccucci, A. Cerri, D. Chakraborty, M.-C. Chen, R. S. Chivukula, G. Cowan, O. Dahl, G. D’Ambrosio, T. Damour, D. de Florian, A. de Gouvêa, T. DeGrand, P. de Jong, G. Dissertori, B. A. Dobrescu, M. D’Onofrio, M. Doser, M. Drees, H. K. Dreiner, D. A. Dwyer, P. Eerola, S. Eidelman, J. Ellis, J. Erler, V. V. Ezhela, W. Fetscher, B. D. Fields, R. Firestone, B. Foster, A. Freitas, H. Gallagher, L. Garren, H.-J. Gerber, G. Gerbier, T. Gershon, Y. Gershtein, T. Gherghetta, A. A. Godizov, M. Goodman, C. Grab, A. V. Griksan, C. Grojean, D. E. Groom, M. Grünewald, A. Gurtu, T. Gutsche, H. E. Haber, C. Hanhart, S. Hashimoto, Y. Hayato, K. G. Hayes, A. Hebecker, S. Heinemeyer, B. Heltsley, J. J. Hernández-Rey, J. Hisano, A. Höcker, J. Holder, A. Holtkamp, T. Hyodo, K. D. Irwin, K. F. Johnson, M. Kado, M. Karliner, U. F. Katz, S. R. Klein, E. Klempt, R. V. Kowalewski, F. Krauss, M. Kreps, B. Krusche, Y. V. Kuyanov, Y. Kwon, O. Lahav, J. Laiho, J. Lesgourgues, A. Liddle, Z. Ligeti, C.-J. Lin, C. Lippmann, T. M. Liss, L. Littenberg, K. S. Lugovsky, S. B. Lugovsky, A. Lusiani, Y. Makida, F. Maltoni, T. Mannel, A. V. Manohar, W. J. Marciano, A. D. Martin, A. Masoni, J. Matthews, U.-G. Meißner, D. Milstead, R. E. Mitchell, B. Mönnig, P. Molaro, F. Moortgat, M. Moskovic, H. Murayama, M. Narain, P. Nason, S. Navas, M. Neubert, P. Nevski, Y. Nir, K. A. Olive, S. Pagan Griso, J. Parsons, C. Patrignani, J. A. Peacock, M. Pennington, S. T. Petcov, V. A. Petrov, E. Pianori, A. Piepke, A. Pomarol, A. Quadt, J. Rademacker, G. Raffelt, B. N. Ratcliff, P. Richardson, A. Ringwald, S. Roesler, S. Rolli, A. Romaniouk, L. J. Rosenberg, J. L. Rosner, G. Rybka, R. A. Ryutin, C. T. Sachrajda, Y. Sakai, G. P. Salam, S. Sarkar, F. Sauli, O. Schneider, K. Scholberg, A. J. Schwartz, D. Scott, V. Sharma, S. R. Sharpe, T. Shutt, M. Siliari, T. Sjöstrand, P. Skands, T. Skwarnicki, J. G. Smith, G. F. Smoot, S. Spanier, H. Spieler, C. Spiering, A. Stahl, S. L. Stone, T. Sumiyoshi, M. J. Syphers, K. Terashi, J. Terning, U. Thoma, R. S. Thorne, L. Tiator, M. Titov, N. P. Tkachenko, N. A. Törnqvist, D. R. Tovey, G. Valencia, R. Van de Water, N. Varelas, G. Venanzoni, L. Verde, M. G. Vincet, P. Vogel, A. Vogt, S. P. Wakely, W. Walkowiak, C. W. Walter, D. Wands, D. R. Ward, M. O. Wascko, G. Weiglein, D. H. Weinberg, E. J. Weinberg, M. White, L. R. Wiencke, S. Willocq, C. G. Wohl, J. Womersley, C. L. Woody, R. L. Workman, W.-M. Yao, G. P. Zeller, O. V. Zenin, R.-Y. Zhu, S.-L. Zhu, F. Zimmermann, P. A. Zyla, J. Anderson, L. Fuller, V. S. Lugovsky, P. Schaffner, Review of Particle Physics, *Phys. Rev. D* 98 (2018) 030001. doi:10.1103/PhysRevD.98.030001. URL <https://link.aps.org/doi/10.1103/PhysRevD.98.030001>
- [51] A. Bialas, M. Gyulassy, Lund Model and an Outside - Inside Aspect of the Inside - Outside Cascade, *Nucl. Phys. B* 291 (1987) 793. doi:10.1016/0550-3213(87)90496-2.
- [52] M. Anselmino, M. Boglione, J. O. Gonzalez Hernandez, S. Melis, A. Prokudin, Unpolarised Transverse Momentum Dependent Distribution and Fragmentation Functions from SIDIS Multiplicities, *JHEP* 04 (2014) 005. arXiv:1312.6261, doi:10.1007/JHEP04(2014)005.
- [53] M. Anselmino, M. Boglione, U. D’Alesio, A. Kotzinian, F. Murgia, A. Prokudin, Role of Cahn and Sivers effects in deep inelastic scattering, *Physical Review D* 71 (7). doi:10.1103/physrevd.71.074006. URL <http://dx.doi.org/10.1103/PhysRevD.71.074006>
- [54] E. L. Berger, F. Coester, Nuclear Effects in Deep Inelastic Lepton Scattering, *Annual Review of Nuclear and Particle Science* 37 (1) (1987) 463–491. arXiv:https://doi.org/10.1146/annurev.ns.37.120187.002335, doi:10.1146/annurev.ns.37.120187.002335. URL <https://doi.org/10.1146/annurev.ns.37.120187.002335>
- [55] D. F. Geesaman, K. Saito, A. W. Thomas, The Nuclear EMC Effect, *Annual Review of Nuclear and Particle Science* 45 (1) (1995) 337–390. arXiv:https://doi.org/10.1146/annurev.ns.45.120195.002005, doi:10.1146/annurev.ns.45.120195.002005. URL <https://doi.org/10.1146/annurev.ns.45.120195.002005>
- [56] L. B. Weinstein, E. Piasetzky, D. W. Higinbotham, J. Gomez, O. Hen, R. Shneor, Short Range Correlations and the EMC Effect, *Physical Review Letters* 106 (5). doi:10.1103/physrevlett.106.052301. URL <http://dx.doi.org/10.1103/PhysRevLett.106.052301>
- [57] P. Ru, Z.-B. Kang, E. Wang, H. Xing, B.-W. Zhang, A global extraction of the jet transport coefficient in cold nuclear matter arXiv:1907.11808.
- [58] X. Guo, J. Qiu, Probing quark-gluon correlation functions, *Physical Review D* 61 (9). doi:10.1103/physrevd.61.096003. URL <http://dx.doi.org/10.1103/PhysRevD.61.096003>

- [59] F. Arleo, S. Peigne, Heavy-quarkonium suppression in p-A collisions from parton energy loss in cold QCD matter, JHEP 03 (2013) 122. [arXiv:1212.0434](#), [doi:10.1007/JHEP03\(2013\)122](#).
- [60] J. L. Albacete, et al., Predictions for  $p$ +Pb Collisions at  $\sqrt{s_{NN}} = 5$  TeV: Comparison with Data, Int. J. Mod. Phys. E25 (9) (2016) 1630005. [arXiv:1605.09479](#), [doi:10.1142/S0218301316300058](#).
- [61] N. Liu, W.-D. Miao, L.-H. Song, C.-G. Duan, Nuclear geometry effect and transport coefficient in semi-inclusive lepton-production of hadrons off nuclei, Phys. Lett. B749 (2015) 88–93. [arXiv:1511.00767](#), [doi:10.1016/j.physletb.2015.07.048](#).

## Supplementary Information

*Color Lifetime in Lund String Model - Struck Quark.* In this supplementary information we derive the Lund String Model (LSM) expression for the color lifetime of the struck quark in first approximation, using massless quarks and treating only the rank-1 hadron that contains the struck quark. Consider a proton of mass  $M$  initially at rest, and an incoming virtual photon in the  $\tilde{z}$  direction. Defining the proton and photon 4-vectors,

$$p = (M, 0, 0, 0) \quad (1)$$

$$q = (\nu, 0, 0, p_{\tilde{z}}) \quad (2)$$

squaring both sides of the latter equation, and defining  $q^2 = -Q^2$ , we can write the virtual photon longitudinal momentum as:

$$p_{\tilde{z}}^2 = \nu^2 + Q^2 \quad (3)$$

We will choose the positive solution of the square root of  $p_{\tilde{z}}$ , and assume that  $Q^2/\nu^2 \ll 1$ :

$$p_{\tilde{z}} = \sqrt{\nu^2 + Q^2} = \nu \sqrt{1 + Q^2/\nu^2} \approx \nu \quad (4)$$

Expressing the dynamics on the light cone, the components  $P^\pm = E \pm p_{\tilde{z}}$  of the total four-momentum vector can be written:

$$P^+ = P_{\text{proton}}^+ + P_{\text{photon}}^+ = M + 2\nu \quad (5)$$

$$P^- = P_{\text{proton}}^- + P_{\text{photon}}^- = M \quad (6)$$

For a hadron  $h$  formed from a  $q\bar{q}$  pair propagating over some space-time distance,  $p_h^+ p_h^- = m^2 + p_\perp^2 \equiv m_\perp^2$ , the variable used in the LSM fragmentation function. The forming hadron carries a fraction  $z$  of the energy-momentum  $P^+$ , such that  $p_h^+ = zP^+$  (see Fig. 1), and thus  $p_h^- = m_\perp^2/(zP^+)$  because the shaded region in the figure has area  $m_\perp^2$ . As is also clear from the figure,  $p_h^- = p_{\text{vertex}}^-$ . The transition from propagating struck quark to forming hadron occurs when a new  $q\bar{q}$  pair is created, the point labeled "vertex" in the plot, and the antiquark becomes part of the leading hadron. The time interval  $T$  and the space interval  $L$  that precede the creation of the vertex can be calculated as follows:

$$p_{\text{vertex}}^+ \equiv E_{\text{vertex}} + p_{z,\text{vertex}} = \kappa(T + L) = (1 - z)P^+ \quad (7)$$

$$p_{\text{vertex}}^- \equiv E_{\text{vertex}} - p_{z,\text{vertex}} = \kappa(T - L) = m_\perp^2/(zP^+) \quad (8)$$

where  $\kappa$  is the LSM string tension, and  $E = \kappa T$  and  $p_{\tilde{z}} = \kappa L$  from the relations  $\frac{dE}{dt} = \kappa$  and  $\frac{dp_{\tilde{z}}}{d\tilde{z}} = \kappa$  for longitudinal coordinate  $\tilde{z}$ .

Solving for  $L$  and using Eq. 5 for  $P^+$ :

$$L = \frac{1}{2\kappa} \left( (1 - z)(M + 2\nu) - \frac{m_\perp^2}{z(M + 2\nu)} \right) \quad (9)$$

If we do not want to make the initial approximation  $\nu \gg Q^2$ , then for the full expression we have:

$$\kappa L = \frac{M}{2} + \nu(1 - z_h) + \frac{1}{2}\nu \left( \sqrt{1 + \frac{Q^2}{\nu^2}} - 1 \right) \quad (10)$$

Finally, in the discussions in this paper, we have used two related forms of the relative energy of a hadron:  $z_h = E_h/\nu$ , which was used in the HERMES papers and which is traditionally used for experimental work, and  $z = \frac{p_h^+}{P^+}$  as written above, which is relevant for calculations on the light cone. The relationship between the two takes the following form:

$$z = \frac{p_h^+}{P^+} = \frac{E_h + p_{h,z}}{M + 2\nu} = z_h \frac{1 + \sqrt{1 - m_\perp^2/(z_h \nu)^2}}{M/\nu + 1 + \sqrt{1 + Q^2/\nu^2}} \quad (11)$$

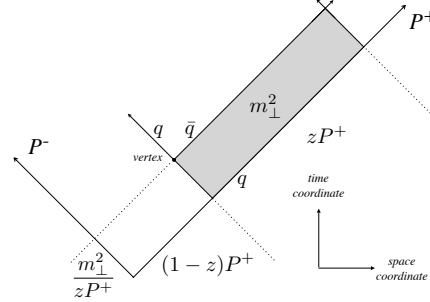


Figure 1: Space-time diagram to illustrate the discussion of this supplementary material. The time axis is vertical in the diagram, while the displacement  $\tilde{z}$  axis is in the horizontal direction. The first vertex is indicated, and the energy-momentum fraction  $z$  of the forming hadron is indicated as a fraction of the total energy-momentum  $P^+$  available from the initial interaction. Formation of the other hadrons is not shown in the figure. Thus, this formula essentially corresponds to the struck quark, in pQCD terminology.